International Journal of Minerals, Metallurgy and Materials
Volume 25, Number 8, August 2018, Page 913
https://doi.org/10.1007/s12613-018-1640-5

Effect of long-term service on the precipitates in P92 steel

Yan-ping Zeng[1)], *Jin-dou Jia*[1)], *Wen-he Cai*[2)], *Shu-qing Dong*[2)], *and Zhi-chun Wang*[2)]

1) School of Materials Science and Engineering; University of Science and Technology Beijing, Beijing 100083, China

2) North China Electric Power Research Institute Co., Ltd., Beijing 100045, China

(Received: 17 January 2018; revised: 21 March 2018; accepted: 23 March 2018)

Abstract: The precipitates in P92 steel after long-term service in an ultra-supercritical unit were investigated by field-emission scanning electron microscopy and transmission electron microscopy and were found to mainly consist of $M_{23}C_6$ carbides, Laves phase, and MX carbonitrides. No Z-phase was observed. $M_{23}C_6$ carbides and Laves phase were found not only on prior austenite grain boundaries, martensite lath boundaries, and subgrain boundaries but also in lath interiors, where two types of MX carbonitrides—Nb-rich and V-rich particles—were also observed but the "winged" complexes were hardly found. Each kind of precipitate within the martensite laths exhibited multifarious morphologies, suggesting that a morphological change of precipitates occurred during long-term service. The $M_{23}C_6$ carbides and Laves phase coarsened substantially, and the latter grew faster than the former. However, MX carbonitrides exhibited a relatively low coarsening rate. The effect of the evolution of the precipitate phases on the creep rupture strength of P92 steel was discussed.

Keywords: precipitate; P92 steel; long-term service; ultra supercritical unit

1. Introduction

One approach to making better use of fossil fuels and reducing CO_2 emissions is to increase the thermal efficiency of fossil-fired power plants by increasing their operating temperatures and pressures [1–4]. Therefore, ultra-supercritical (USC) power plants with improved thermal efficiency have been built over the past several decades [5–7]. However, heat-resistant materials with high creep rupture strength are required for these more demanding service conditions. P92 steel has been recognized as an excellent ferritic heat-resistant steel for USC boilers because it exhibits high creep rupture strength, excellent thermal conductivity, a low coefficient of thermal expansion, and good processability accompanied by satisfactory resistance to stress corrosion cracking and oxidation [8–10]. The second-phase particles play an important role in enhancing the creep resistance of this steel [11–13]. The precipitate phases in normalized and tempered P92 steel primarily consist of $M_{23}C_6$ carbides and MX carbonitrides [2–3,14]. The coarsening of these phases, together with the formation and growth of new secondary phases (i.e., Laves phase and Z-phase) during service, would result in a substantial decrease in creep resistance of the steel [15–19]. Studying the evolution of these precipitate phases under real operating conditions as well as under various aging or creep conditions is vitally important [20–24] because the stress (or strain) level clearly influences the formation and growth of the precipitate phases [8,17,24–25]. Hence, the objective of this paper is to provide a deeper understanding of the precipitate phases in P92 steel after long-term service in a USC unit.

2. Experimental

The material used for this study is a hot reheat steam pipe of a USC boiler with an internal diameter of 502 mm and wall thickness of 32 mm; it has been in service for 9854 h at a temperature of 603°C and a pressure of 5.87 MPa. The pipe was initially normalized at 1070°C and subsequently tempered at 770°C; its chemical composition is given in Table 1. Metallographic specimens were cut from the pipe and were chemically etched in a solution of 5 g of iron(III) chloride in 100 mL of distilled water mixed with 50 mL of concentrated hydrochloric acid. These samples were then examined by Zeiss Supra 55 field-emission scanning electron microscopy (FESEM). Thin foils and extraction carbon rep-

Corresponding author: Yan-ping Zeng E-mail: zengyanping@mater.ustb.edu.cn

licas were prepared by the twin-jet electropolishing technique in an electrolyte of 5vol% perchloric acid + 95vol% ethanol with a current of 25–30 mA at −30°C and by the method described in the literature [26]. They were then observed in a JEM-2100 transmission electron microscope operated at 200 kV. The precipitate phases were identified by energy-dispersive X-ray spectrometry (EDS) and selected-area electron diffraction (SAED), and their sizes were measured from transmission electron microscopy (TEM) micrographs using the Image-Pro Plus software.

Table 1. Chemical composition of the investigated pipe wt%

C	Si	Mn	S	P	Cr	Ni	Mo	W	V	Nb	B	Al	N	Fe
0.10	0.30	0.43	0.0016	0.012	8.47	0.15	0.33	1.45	0.20	0.066	0.0017	0.0078	0.037	Balance

3. Results

3.1. Precipitates on the boundaries

SEM microstructure of the investigated pipe is shown in Fig. 1, which consists of tempered martensite laths. Second-phase particles of various sizes are present not only at prior austenite grain boundaries (PAGBs), martensite lath boundaries, and subgrain boundaries but also in lath interiors. The particles distributed at martensite lath boundaries make the morphology of lath martensite clearly visible.

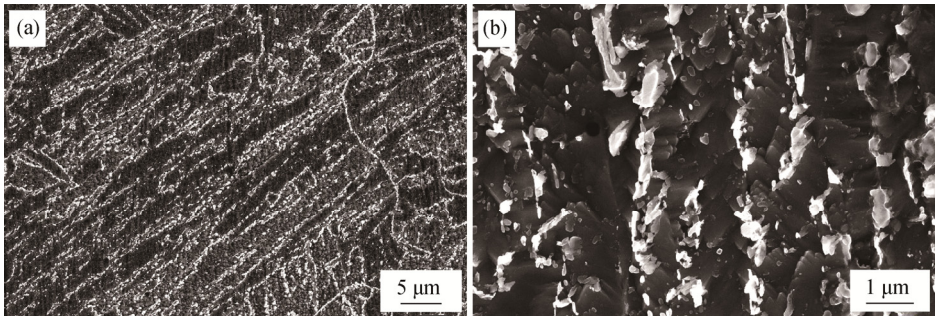

Fig. 1. Microstructures of the investigated pipe, as observed by SEM: (a) lower magnification image; (b) higher magnification image.

Fig. 2(a) is a typical bright-field TEM image showing block-like precipitate phases with an irregular shape and an average size of the order of 200 nm at PAGBs, lath boundaries, and subgrain boundaries. They are often found as clusters along the boundaries. Stripes are observed in some of particles, implying that stacking faults were formed in them [25,27]. The EDS spectra indicate that the levels of tungsten and molybdenum in the particles with stripes (44.34wt% and 12.26wt%, Fig. 2(b)) are substantially greater than those in the matrix (0wt% and 0wt%, Fig. 2(d)) and they should have a hexagonal crystal structure based on SAED analysis (Fig. 2(e)). Thus, these particles are determined to be intermetallic Laves phase $(Fe,Cr)_2(W,Mo)$. However, the analysis of the particles without stripes by EDS and SAED reveals that they are rich in Cr (55.31wt% and 7.95wt%, respectively, for the particle and matrix, see Figs. 2(c) and 2(d)) and exhibit a face-centered-cubic crystal structure (Fig. 2(f)). Therefore, these particles are identified as $M_{23}C_6$ carbides containing Fe along with a small amount of W and Mo. This result indicates that two kinds of precipitate phases—Laves phase and $M_{23}C_6$ carbides—are present at PAGBs, lath boundaries, and subgrain boundaries. Characteristic streaks on the SAED pattern of the Laves-phase particles are observed (Fig. 2(e)), similar to the result observed previously in 9%–12% Cr steel [28–29]. This feature enables easy distinction between the Laves phase and the $M_{23}C_6$ carbides.

3.2. Precipitates within martensite laths

Figs. 3(a) and 3(b) are TEM micrographs of a carbon extraction replica sample, revealing the precipitate phases within martensite laths. Two kinds of secondary particles with different contrast levels are clearly observed. The dark-colored particles, which were determined to be Laves phase by analysis of the EDS spectra and SAED patterns (Figs. 3(c) and 3(e)), exhibit three different morphologies: sphere-like (particles A1 and A2), short rod-like (particles A3 and A4), and irregular block-like (particles A5–A7). This observation differs from previously reported results [2,7] that showed only block-like Laves phases were formed in P92 steel crept for up to 9755 h at 600°C and under 160 MPa and were distributed merely on PAGBs, lath boundaries, and subgrain boundaries. The detected spherical particles have a diameter of approximately 80–160 nm. Short rod-like particles are approximately 300–360 nm in length and 80–140 nm in width, and block-like particles with sizes

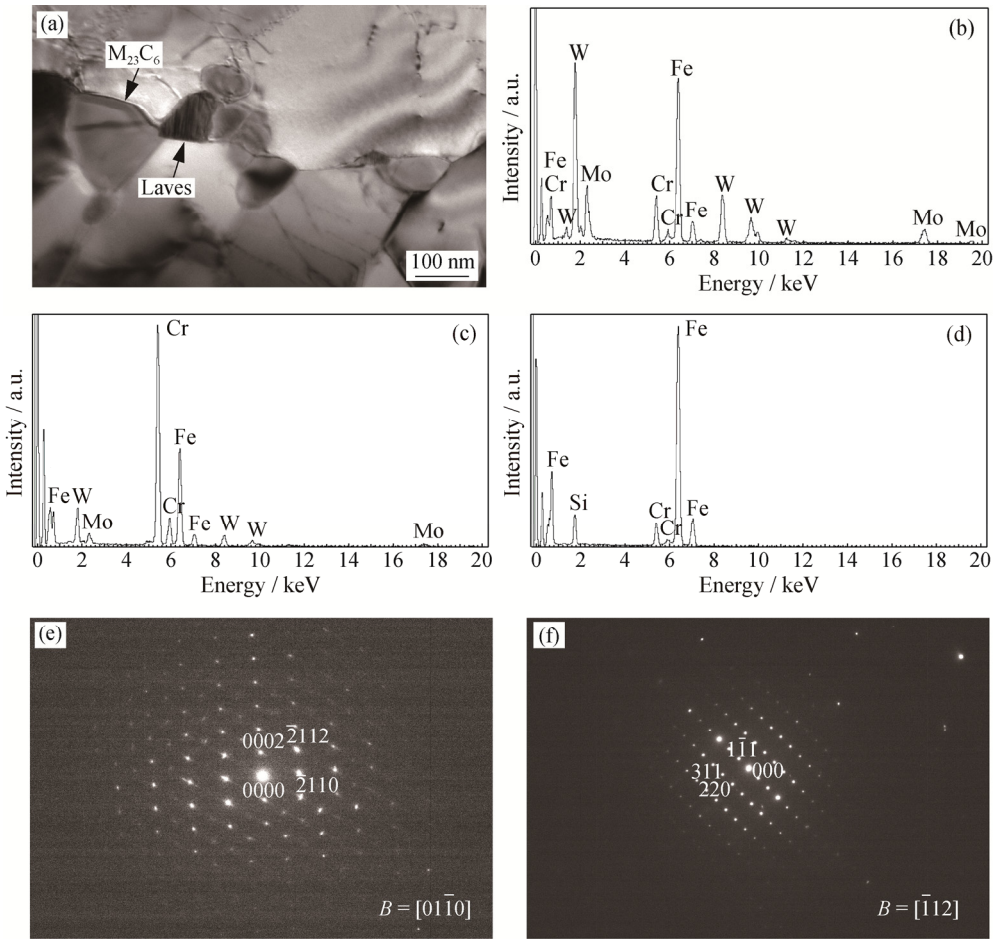

Fig. 2. Secondary particles at prior austenite grain boundaries, martensite lath boundaries, and subgrain boundaries: (a) TEM bright-field image; (b, c) EDS spectra of the particles with (b) and without (c) stripes indicated by arrows in Fig. 2(a); (d) EDS spectrum of the matrix; (e, f) SAED patterns of the particles with (e) and without (f) stripes indicated by arrows in Fig. 2(a).

ranging from 80 to 360 nm in diameter. These Laves phases are often located close to the light-colored secondary particles, which are identified as $M_{23}C_6$ carbides through analysis of EDS spectra and SAED patterns (Figs. 3(d) and 3(f)). The $M_{23}C_6$ carbides also exhibit multifarious morphologies such as sphere-like (particles B1 and B2), short rod-like (particles B3 and B4), rectangle-like (particles B5 and B6), rhombus-like (particles B7 and B8), and irregular block-like (particles B9 and B10). This observation also differs from previously reported results [8,15] that only spheroidal and rod-shaped particles were observed in T/P92 steel aged at 650°C for 5000 h or crept for 12480 h at 600°C and under 160 MPa and were mainly located on PAGBs, lath boundaries, and subgrain boundaries. The detected spherical $M_{23}C_6$ carbides have a diameter of approximately 30–120 nm. Rectangle-like $M_{23}C_6$ carbides have dimensions of approximately 30–100 nm in length and 20–60 nm in width. Rhombus-like $M_{23}C_6$ carbides have a side length of approximately 40–80 nm. Short rod-like $M_{23}C_6$ carbides have a dimension of approximately 30–230 nm in length and 15–100 nm in width, and block-like $M_{23}C_6$ carbides have a diameter ranging from 80 to 320 nm. This diameter is much larger than the size of $M_{23}C_6$ carbides in P92 steel normalized at 1070°C for 2 h and then tempered at 775°C for 2 h [2,14], implying that $M_{23}C_6$ carbides coarsened substantially under actual service conditions. The average size of Laves phases is larger than that of $M_{23}C_6$ carbides with the same morphology. Because the Laves phase formed long after the $M_{23}C_6$ carbide in the steel [2,8,15], the Laves phase must grow faster than the $M_{23}C_6$ carbide.

Moreover, two kinds of very fine particles were also found in the lath interiors (Figs. 4(a)–4(d) and 5(a)–5(d)). Analysis of EDS spectra and SAED patterns revealed that these particles are rich in Nb and V (Fig. 4(e)) or V and Nb (Fig. 5(e)) and have a face-centered-cubic crystal structure (Figs. 4(f) and 5(f)). Hence, they are determined to be (Nb,V)-rich and (V,Nb)-rich MX carbonitrides, respectively.

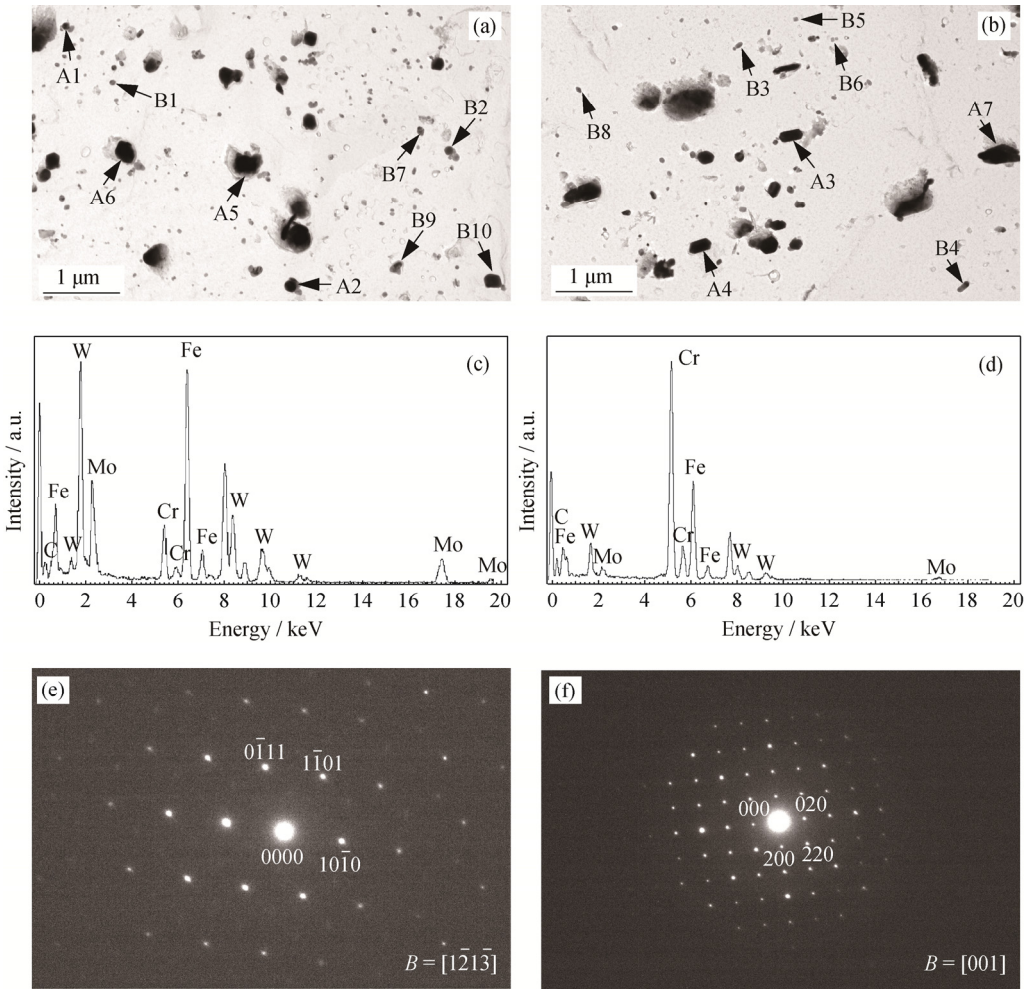

Fig. 3. Secondary particles within martensite laths: (a, b) TEM micrographs of the carbon replica; (c,d) EDS spectra of particles A6 (c) and B10 (d); (e,f) SAED patterns of particles A6 (e) and B10 (f).

As shown in Figs. 4(a)–4(d), (Nb,V)-rich particles mainly exhibit sphere-like morphology (particles C1–C3); however, the particles of other shapes, such as plate-like (particle C4), square-like (particle C5), and irregular block-like (particle C6), are also observed. The detected spherical particles have a diameter of approximately 30–60 nm. Plate-like particles have a length and width of approximately 60–130 nm and 40–70 nm, respectively. Square-like particles have a side length of approximately 110 nm, and block-like particles have a diameter of approximately 80 nm.

The (V,Nb)-rich particles also exhibit various morphologies (Figs. 5(a)–5(d)), including sphere-like (particle D1), oval-like (particles D2 and D3), rectangle-like (particles D4–D7), hexagonal-like (particle D8), irregular block-like (particles D9 and D10), and plate-like (particles D11 and D12). The detected spherical particles have a diameter of approximately 10–40 nm. Oval-like particles have a major-axis length of approximately 50–100 nm and a minor-axis length of approximately 30–60 nm. Rectangle-like particles have a length and width of approximately 40–150 nm and 20–90 nm, respectively. Hexagonal-like particles have an average side length of approximately 60 nm. Irregular block-like particles have a size ranging from 30 to 100 nm in diameter, and plate-like particles have dimensions of approximately 40–120 nm in length and 20–40 nm in width. These results differ from previous reports [2,14] that MX carbonitrides exhibited only three different morphologies in P92 steel normalized at 1070°C for 2 h followed by tempering at 715–835°C for 2 h: spheroidal Nb-rich carbonitrides, plate-like V-rich nitrides, and "winged" particles consisting of Nb-rich carbonitrides in the core and V-rich carbonitrides on both sides. The mean sizes of these particles were obviously smaller than that of the MX carbonitrides in the present study, suggesting that not only coarsening but also a morphological change of MX carbonitrides occurred during long-term service.

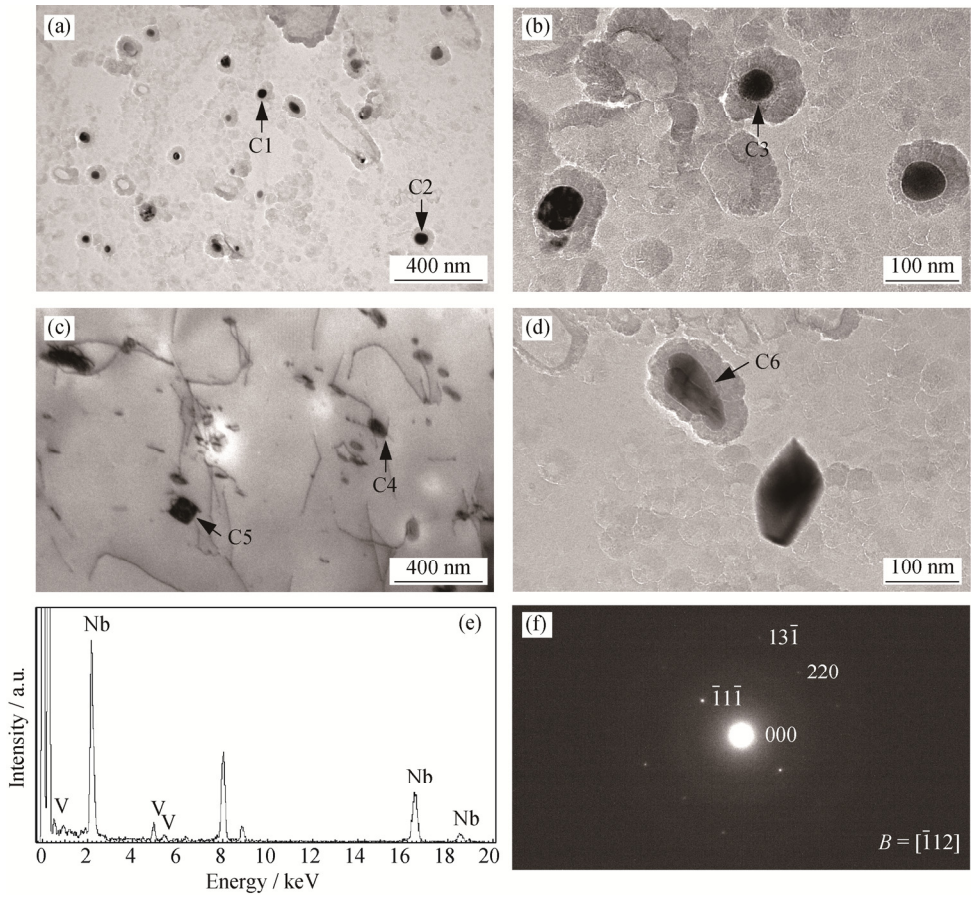

Fig. 4. (Nb,V)-rich MX carbonitride in lath interiors: (a–d) TEM micrographs; (e) EDS spectrum of particle C1; (f) SAED pattern of particle C1.

4. Discussion

The excellent mechanical properties of P92 steel are attributed to the martensitic microstructure, which consists of martensite lath, block, and packets with a high dislocation density and a dispersive distribution of fine precipitate particles [16]. The second-phase particles play an important role in the creep behavior of such steel.

The precipitates in normalized and tempered P92 steel are primarily composed of $M_{23}C_6$ carbides and MX carbonitrides [8,15,21]. Laves phase is not present in this state because the tempering temperature is above its solution temperature [30]. Fine MX carbonitrides are mainly distributed within martensite laths [10] and suppress the gliding of dislocations toward lath and block boundaries, which reduces the number of annihilated dislocations; by contrast, $M_{23}C_6$ carbides are decorated on PAGBs, lath boundaries, and subgrain boundaries [7,11] and prevent the climbing and redistribution of dislocations in the boundary wall, which not only decreases the efficiency of dislocation absorption by the boundaries and the number of annihilated dislocations but also effectively hinders the migration of lath boundaries. This effect stabilizes free dislocations and the subgrain structure against recovery and further enhances the dislocation hardening and sub-boundary hardening, which is inversely proportional to the width of laths and blocks [16]. However, the coarsening of $M_{23}C_6$ carbides by the mechanism of Ostwald ripening during long-term service reduces their ability to prevent migration of the lath boundaries by the motion and unknitting of dislocations forming lath boundaries [31–32]. This coarsening hence accelerates the widening of lath or block and its evolution into subgrains, resulting in the loss of sub-boundary hardening. The creep rate versus time curves for tempered martensitic 9% Cr steels consist of a primary or transient creep region and of a tertiary or acceleration creep region. The creep rate decreases with time in the transient creep region. After reaching a minimum value, the creep rate increases with time in the acceleration creep region [33]. Abe *et al.* [31,34] have shown that the transient creep is basically a consequence of the movement and annihilation of high-density dislocations produced by martensitic transformation during cooling after normalizing and that the acceleration creep is a consequence of the gradual loss of creep rupture strength

via the coarsening of lath or block by the migration of boundaries accompanied by the absorption of excess dislocations from lath or block interiors. Notably, the soluble boron retards the Ostwald ripening of $M_{23}C_6$ carbides near PAGBs during creep by enrichment into the carbides, which effectively stabilizes the lath martensitic microstructure and improves the creep rupture strength of 9% Cr steels [16,33].

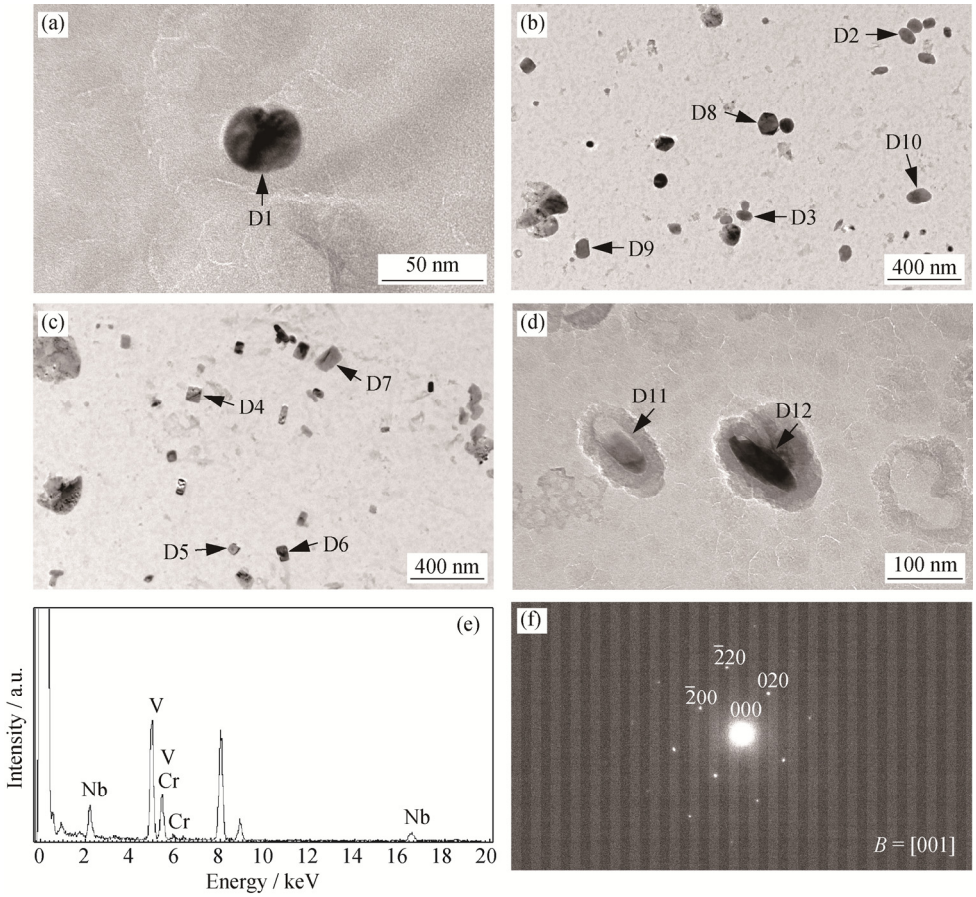

Fig. 5. (V,Nb)-rich MX carbonitrides in lath interiors: (a–d) TEM micrographs; (e) EDS spectrum of particle D1; (f) SAED pattern of particle D1.

The addition of tungsten (W) and molybdenum (Mo) to 9% Cr steels increases the creep resistance of the steels. The beneficial effects of W and Mo on the creep rupture strength are generally considered to be due to solid-solution strengthening [35]. However, the precipitation of Laves phase during service results in the depletion of W and Mo from the solid solution. Although this depletion leads to a deterioration of solid-solution strengthening, fine Laves-phase particles produce a substantial precipitation strengthening effect in the early stages of precipitation [15,36]. The formation of fine Laves phase at PAGBs, lath boundaries, and subgrain boundaries also reduces the efficiency of dislocation absorption by the boundaries and effectively inhibits the migration of lath boundaries, which further enhances the dislocation hardening and sub-boundary hardening [2,32]. In addition, the precipitation of Laves phase, removing W and Mo from solid solution, has a positive effect on the coarsening stability of $M_{23}C_6$ carbides, which is mainly controlled by the content of the substitutional elements, such as W and Mo, in the matrix [36–37]. Thus, in general, the creep rupture strength of the steel at the beginning increases with the precipitation of fine Laves-phase particles, reaches a peak, and then decreases because of fast growth of this phase, as described in the literature [8]. Reducing the coarsening rate of Laves phase is important for preserving the good creep resistance of the steel. Alloying elements can positively influence the coarsening behavior of Laves phase. For example, the addition of Co decreases the diffusion rates of solute atoms [38], which slows the Ostwald ripening of both $M_{23}C_6$ carbides and Laves phase [24,39].

With regard to the nucleation and growth of Laves phase in P92 steel, two mechanisms have been reported [25,27]. One is that Laves-phase particles nucleate on martensite lath

boundaries or subgrain boundaries with no $M_{23}C_6$ carbides in the vicinity and are coherent with the grains on one side of the boundaries. They grow into the grains on the other side of the boundaries with which they do not have a rational orientation relationship because incoherent interfaces are more mobile than coherent interfaces. In the second mechanism, Laves phases precipitate in the chromium-depleted regions adjacent to $M_{23}C_6$ carbides because such regions have relatively high W and Mo contents, which is beneficial to the formation of Laves phase. Laves phases grow at the expense of the $M_{23}C_6$ carbides in the vicinity because of the rearrangement of the alloy elements such as Cr, W, and Mo. Thus, Laves phases are often located near $M_{23}C_6$ carbides.

As previously mentioned, the fine MX carbonitrides in lath interiors act as obstacles to dislocation movement to lath and block boundaries, which reduces the number of annihilated dislocations and decreases the creep rate. In particular, the "winged" particles, which are formed by the undissolved and spheroidal Nb-rich carbonitrides during normalization as nucleation sites for the plate-like V-rich carbonitrides during tempering [2,14], play important roles in the strengthening effect of precipitates [40]. On the one hand, mobile dislocations would be considerably trapped at the concavity of the V-wings during creep deformation; thus, the "winged" complexes can restrain dislocation climbing even under conditions where a dislocation climbs over a spherical precipitate. On the other hand, the V-wings are sure to pin mobile dislocations more strongly than spherical precipitates because the probability of dislocation trapping at the V-wings is larger than that at spherical precipitates. Therefore, the V-wings restrain dislocation pile-up on grain boundaries, which lead to grain-boundary sliding and delay the change of the creep deformation mechanism from transgranular dislocation sliding to grain-boundary sliding. However, the "winged" particles were hardly found in the investigated pipe and the reasons for this require further investigation. The lack of the "winged" complexes would possibly decrease the creep resistance of the pipe.

Z-phase Cr(V,Nb)N is thermodynamically the most stable nitride in most of the new 9%–12% Cr steels [41]. Z-phase precipitation occurs after an extended time at the service temperature [42]. MX carbonitrides are preferred nucleation sites for Z-phase because of the existence of the semi-coherent interface between them, which reduces the interfacial energy. Z-phase nucleates on existing MX particles via the diffusion of Cr from the matrix into MX [43–45]. After a Z-phase particle has nucleated, it can grow quickly by consuming the MX carbonitride adjacent to it. Thus, Z-phase particles are usually very large and do not contribute to precipitation hardening [46]. Instead, the Z-phase can completely dissolve the beneficial MX carbonitrides, resulting in an MX-precipitate-free zone around a Z-phase particle, which is responsible for a decrease in the creep rupture strength of 9%–12% Cr steels [36,43]. Cr strongly influences the kinetics of Z-phase precipitation [41]. Specifically, Z-phase formation can be delayed by reducing the Cr content [47]. The rate of Z-phase precipitation in 9% Cr steels is extremely low [46]. Consequently, no Z-phase was observed in the investigated pipe. Nb accelerates Z-phase formation because Nb enhances the interfacial energy between (V,Nb)N and ferrite, which is reduced by incorporation of Cr into the lattice of (V,Nb)N [48–49].

5. Conclusions

(1) The precipitates in P92 steel after long-term service in a USC unit mainly consist of $M_{23}C_6$ carbides, Laves phase, and MX carbonitrides. No Z-phase is observed.

(2) $M_{23}C_6$ carbides are found not only on PAGBs, lath boundaries, and subgrain boundaries but also in lath interiors, where $M_{23}C_6$ carbides exhibit multifarious morphologies and are coarsened heavily.

(3) Laves-phase particles precipitate inside martensite laths as well as on PAGBs, lath boundaries, and subgrain boundaries. Stripes are observed in some of the particles on the boundaries, implying that stacking faults were formed in them. The Laves phases within martensite laths exhibit three different morphologies, and their average sizes are larger than that of $M_{23}C_6$ carbides with the same morphology, indicating that the Laves phase grows faster than the $M_{23}C_6$ carbide because the Laves phase forms long after the $M_{23}C_6$ carbide.

(4) Two types of MX carbonitrides—Nb-rich and V-rich particles—are observed in lath interiors. Both exhibit multifarious morphologies and are obviously coarsened. The winged particles are hardly found, and the reasons for this lack of winged particles warrant further investigation.

(5) The effect of the evolution of the precipitate phases on creep rupture strength was discussed.

References

[1] F. Masuyama, History of power plants and progress in heat resistant steels, *ISIJ Int.*, 41(2001), No. 6, p. 612.

[2] P.J. Ennis, A. Zielinska-lipiec, O. Wachter, and A. Czyrska-filemonowicz, Microstructural stability and creep rupture strength of the martensitic steel P92 for advanced power plant, *Acta Mater.*, 45(1997), No. 12, p. 4901.

[3] P.J. Ennis, A. Zielińska-Lipiec, and A. Czyrska-Filemonowicz,

Influence of heat treatments on microstructural parameters and mechanical properties of P92 steel, *Mater. Sci. Technol.*, 16(2000), No. 10, p. 1226.

[4] L. Zhao, H.Y. Jing, J.J. Xiu, Y.D. Han, and L.Y. Xu, Experimental investigation of specimen size effect on creep crack growth behavior in P92 steel welded joint, *Mater. Des.*, 57(2014), p. 736.

[5] R. Viswanathan, K. Coleman, and U. Rao, Materials for ultra-supercritical coal-fired power plant boilers, *Int. J. Press. Vessels Pip.*, 83(2006), No. 11-12, p. 778.

[6] J. Cao, Y. Gong, Z.G. Yang, X.M. Luo, F.M. Gu, and Z.F. Hu, Creep fracture behavior of dissimilar weld joints between T92 martensitic and HR3C austenitic steels, *Int. J. Press. Vessels Pip.*, 88(2011), No. 2-3, p. 94.

[7] J. Jiang, L.H. Zhu, and Y.F. Wang, Hardness variation in P92 heat-resistant steel based on microstructural evolution during creep, *Steel Res. Int.*, 84(2013), No. 8, p. 732.

[8] M. Nie, J. Zhang, F. Huang, J.W. Liu, X.K. Zhu, Z.L. Chen, and L.Z. Ouyang, Microstructure evolution and life assessment of T92 steel during long-term creep, *J. Alloys Compd.*, 588(2014), p. 348.

[9] T. Sakthivel, M. Vasudevan, K. Laha, P. Parameswaran, K.S. Chandravathi, S.Panneer Selvi, V. Maduraimuthu, and M.D. Mathew, Creep rupture behavior of 9Cr–1.8W–0.5Mo–VNb (ASME grade 92) ferritic steel weld joint, *Mater. Sci. Eng. A*, 591(2014), p. 111.

[10] D.R. Barbadikar, A.R. Ballal, D.R. Peshwe, J. Ganeshkumar, K. Laha, and M.D. Mathew, A study on the effect of tempering temperature on tensile properties of P92 steel by automated ball indentation technique, *Procedia Eng.*, 86(2014), p. 910.

[11] Y.Z. Shen, H. Liu, Z.X. Shang, and Z.Q. Xu, Precipitate phases in normalized and tempered ferritic/martensitic steel P92, *J. Nucl. Mater.*, 465(2015), p. 373.

[12] A. Kostka, K.G. Tak, R.J. Hellmig, Y. Estrin, and G. Eggeler, On the contribution of carbides and micrograin boundaries to the creep strength of tempered martensite ferritic steels, *Acta Mater.*, 55(2007), No. 2, p. 539.

[13] K. Maile, Evaluation of microstructural parameters in 9–12% Cr-steels, *Int. J. Press. Vessels Pip.*, 84(2007), No. 1-2, p. 62.

[14] A. Zielińska-Lipiec, A. Czyrska-Filemonowicz, P.J. Ennis, and O. Wachter, The influence of heat treatments on the microstructure of 9% chromium steels containing tungsten, *J. Mater. Process. Technol.*, 64(1997), No. 1-3, p. 397.

[15] X.F. Guo, J.M. Gong, Y. Jiang, and D.S. Rong, The influence of long-term aging on microstructures and static mechanical properties of P92 steel at room temperature, *Mater. Sci. Eng. A*, 564(2013), p. 199.

[16] F. Abe, Precipitate design for creep strengthening of 9% Cr tempered martensitic steel for ultra-supercritical power plants, *Sci. Technol. Adv. Mater.*, 9(2008), No. 1, art. No. 013002.

[17] K. Sawada, K. Kubo, and F. Abe, Creep behavior and stability of MX precipitates at high temperature in 9Cr–0.5Mo–1.8W–VNb steel, *Mater. Sci. Eng. A*, 319-321(2001), p. 784.

[18] J.S. Lee, H. Ghassemi Armaki, K. Maruyama, T. Muraki, and H. Asahi, Causes of breakdown of creep strength in 9Cr–1.8W–0.5Mo–VNb steel, *Mater. Sci. Eng. A*, 428(2006), No. 1-2, p. 270.

[19] H.K. Danielsen and J. Hald, Behaviour of Z phase in 9–12%Cr steels, *Energy Mater.*, 1(2006), No. 1, p. 49.

[20] M. Hattestrand, M. Schwind, and H.O. Andrén, Microanalysis of two creep resistant 9–12% chromium steels, Mater. *Sci. Eng. A*, 250(1998), No. 1, p. 27.

[21] K. Rodak, A. Hernas, and A. Kielbus, Substructure stability of highly alloyed martensitic steels for power industry, *Mater. Chem. Phys.*, 81(2003), No. 2-3, p. 483.

[22] H. Cerjak, P. Hofer, and B. Schaffernak, The influence of microstructural aspects on the service behaviour of advanced power plant steels, *ISIJ Int.*, 39(1999), No. 9, p. 874.

[23] M. Yoshizawa, M. Igarashi, K. Moriguchi, A. Iseda, H.G. Armaki, and K. Maruyama, Effect of precipitates on long-term creep deformation properties of P92 and P122 type advanced ferritic steels for USC power plants, *Mater. Sci. Eng. A*, 510-511(2009), p. 162.

[24] A. Fedoseeva, N. Dudova, and R. Kaibyshev, Creep strength breakdown and microstructure evolution in a 3%Co modified P92 steel, *Mater. Sci. Eng. A*, 654(2016), p. 1.

[25] H.R. Cui, F. Sun, K. Chen, L.T. Zhang, R.C. Wan, A.D. Shan, and J.S. Wu, Precipitation behavior of Laves phase in 10%Cr steel X12CrMoWVNbN10-1-1 during short-term creep exposure, *Mater. Sci. Eng. A*, 527(2010), No. 29-30, p. 7505.

[26] Y.Z. Shen, S.H. Kim, C.H. Han, H.D. Cho, W.S. Ryu, and C.B. Lee, Vanadium nitride precipitate phase in a 9% chromium steel for nuclear power plant applications, *J. Nucl. Mater.*, 374(2008), No. 3, p. 403.

[27] O. Prat, J. Garcia, D. Rojas, G. Sauthoff, and G. Inden, The role of Laves phase on microstructure evolution and creep strength of novel 9%Cr heat resistant steels, *Intermetallics*, 32(2013), p. 362.

[28] Q. Li, Precipitation of Fe_2W Laves phase and modeling of its direct influence on the strength of a 12Cr–2W steel, *Metall. Mater. Trans. A*, 37(2006), No. 1, p. 89.

[29] K. Yamamoto, Y. Kimura, and Y. Mishima, Effect of matrix microstructure on precipitation of Laves phase in Fe–10Cr–1.4W(–Co) alloys, *Intermetallics*, 14(2006), No. 5, p. 515.

[30] G. Dimmler, P. Weinert, E. Kozeschnik, and H. Cerjak, Quantification of the Laves phase in advanced 9–12% Cr steels using a standard SEM, *Mater. Charact.*, 51(2003), No. 5, p. 341.

[31] F. Abe, Coarsening behavior of lath and its effect on creep rates in tempered martensitic 9Cr–W steels, *Mater. Sci. Eng. A*, 387-389(2004), p. 565.

[32] K. Sawada, M. Takeda, K. Maruyama, R. Ishii, M. Yamada, Y. Nagae, and R. Komine, Effect of W on recovery of lath structure during creep of high chromium martensitic steels, *Mater. Sci. Eng. A*, 267(1999), No. 1, p. 19.

[33] F. Abe, T. Horiuchi, M. Taneike, and K. Sawada, Stabiliza-

tion of martensitic microstructure in advanced 9Cr steel during creep at high temperature, *Mater. Sci. Eng. A*, 378(2004), No. 1-2, p. 299.

[34] F. Abe, S. Nakazawa, H. Araki, and T. Noda, The role of microstructural instability on creep-behavior of a martensitic 9Cr–2W steel, *Metall. Trans. A*, 23(1992), No. 2, p. 469.

[35] K. Maruyama, K. Sawada, and J.-I. Koike, Strengthening mechanisms of creep resistant tempered martensitic steel, *ISIJ Int.*, 41(2001), No. 6, p. 641.

[36] J. Hald, Microstructure and long-term creep properties of 9-12% Cr steels, *Int. J. Press. Vessels Pip.*, 85(2008), No. 1-2, p. 30.

[37] J. Hald, L. Korcakova, H.K. Danielsen, and K.V. Dahl, Thermodynamic and kinetic modeling: creep resistant materials, *Mater. Sci. Technol.*, 24(2008), No. 2, p. 149.

[38] Å. Gustafson and J. Ågren, Possible effect of Co on coarsening of M23C6 carbide and Orowan stress in a 9% Cr steel, *ISIJ Int.*, 41(2001), No. 4, p. 356.

[39] A. Kipelova, M. Odnobokova, A. Belyakov, and R. Kaibyshev, Effect of Co on creep behavior of a P911 steel, *Metall. Mater. Trans. A*, 44(2013), No. 1, p. 577.

[40] K. Hamada, K. Tokuno, Y. Tomita, H. Mabuchi, and K. Okamoto, Effects of precipitate shape on high temperature strength of modified 9Cr–1Mo steels, *ISIJ Int.*, 35(1995), No. 1, p. 86.

[41] H.K. Danielsen and J. Hald, A thermodynamic model of the Z-phase Cr(V, Nb)N, *Calphad*, 31(2007), No. 4, p. 505.

[42] K. Sawada, H. Kushima, and K. Kimura, Z-phase formation during creep and aging in 9–12% Cr heat resistant steels, *ISIJ Int.*, 46(2006), No. 5, p. 769.

[43] A. Golpayegani, H.O. Andrén, H. Danielsen, and J. Hald, A study on Z-phase nucleation in martensitic chromium steels, *Mater. Sci. Eng. A*, 489(2008), No. 1-2, p. 310.

[44] H.K. Danielsen and J. Hald, On the nucleation and dissolution process of Z-phase Cr(V, Nb)N in martensitic 12%Cr steels, *Mater. Sci. Eng. A*, 505(2009), No. 1-2, p. 169.

[45] X.S. Zhou, Y.C. Liu, C.X. Liu, L.M. Yu, and H.J. Li, Formation and evolution of precipitates in high Cr ferritic heat-resistant steels, *Mater. Res. Innovations*, 19(2015), No. S4, p. S193.

[46] J. Hald and H.K. Danielsen, Z-phase strengthened martensitic 9–12%Cr steels, [in] *Proceedings of 3rd Symposium on Heat Resistant Steels and Alloys for High Efficiency USC Power Plants*, *Tsukuba*, 2009, p. 1.

[47] H.K. Danielsen, P.E. Di Nunzio, and J. Hald, Kinetics of Z-phase precipitation in 9 to 12 pct Cr steels, *Metall. Mater. Trans. A*, 44(2013), No. 5, p. 2445.

[48] K.H. Lee, S.M. Hong, J.H. Shim, J.Y. Suh, J.Y. Huh, and W.S. Jung, Effect of Nb addition on Z-phase formation and creep strength in high-Cr martensitic heat-resistant steels, *Mater. Charact.*, 102(2015), p. 79.

[49] L. Cipolla, H.K. Danielsen, P.E. Di Nunzio, D. Venditti, J. Hald, and M.A.J. Somers, On the role of Nb in Z-phase formation in a 12% Cr steel, *Scripta Mater.*, 63(2010), No. 3, p. 324.